Characterizing the Mechanisms of Ultrasound RF Time Series-Based Tissue Classification

By

KEVIN MULTANI
CONRAD NG
KEVIN SHEN

Engineering Physics 459
Department of Engineering Physics
UNIVERSITY OF BRITISH COLUMBIA

A proposal submitted to Engineering Physics Instructors in accordance with the requirements of the course ENPH459 in the Department of Engineering Physics.

DECEMBER 17, 2015

PROJECT NUMBER: 1608

Executive Summary

Ultrasound technology has the potential to efficiently and non-invasively detect malignant cancer tumors. Existing cancer diagnosis techniques such as Magnetic Resonance Imaging (MRI) are prone to generating false-positives, and other traditional techniques can be uncomfortably invasive. This document contains a proposal to investigate hypothesized mechanisms that drive a new time-series Prostate Cancer imaging technique using ultrasound. Replacing conventional diagnoses with this time-series based ultrasound technique will not only improve early-diagnosis rate, but also be easily integrated into hospitals with existing ultrasound infrastructure.

The primary goal of the project is to investigate and identify the mechanical properties of tissue samples and ultrasound probes that allow ultrasound time-series analysis to accurately classify tissue types. In particular, how microvibration interaction between tissue samples and ultrasound probes affects tissue classification accuracy will be explored.

This proposal provides background information and defines the goals over the timeline of the project from January to April. Experiments will be designed to test and analyze the microvibration phenomenon using Philips Ultrasound Phantom machines. The Philips machines are specially-made phantoms provided by Philips Research North America and experiments will place these phantoms with varying mechanical properties such as elasticity and scatterer density under controlled microvibration experiments. In parallel, software packages including Field-II, k-Wave, and COMSOL/ANSYS will be used to match the conditions of the planned experiments and predict results. Simulation data will be cross referenced against experimental results to develop a better understanding of the data and sources of information. After conducting the experiments and simulations, we will document our findings in written publication.

Table of Contents

List of Tables

List of Figures

CHAPTER 1

INTRODUCTION

The following chapter of this proposal outlines the motivation, background, and objectives in the characterization of ultrasound-based tissue classification. The primary motivation for this project is to contribute to the work of Dr. Purang Abolmaesumi (project sponsor), his team, and Phillips Research North America to develop a new Ultrasound-based Prostate Cancer detection technique. The background described in this chapter will focus on concepts related to the proposed set of solutions: prostate cancer overview, ultrasound interactions, ultrasound imaging and characteristics, bio-heat diffusion, mechanical properties of tissue, and simulation tools. Lastly, the section will conclude with a detailed description of this project's objectives and goals.

1.1 Motivation

Prostate Cancer is the most common cancer among Canadian men. It is the third leading cause of death from cancer in men in Canada. According to the Canadian Cancer Society, it is estimated that 24,000 (representing 24% of new cancer cases) men will be diagnosed with prostate cancer, of which 4,100 will die. These numbers, however, are likely to double by 2025, when the baby boomer generation will reach the age of peak prevalence. If the diagnosis is prompt, the five-year survival rate can be over 95% [www.cancer.ca].

Early diagnosis and accurate staging of prostate cancer enables treatment options that cater to the patient: surgery, ablation, and radiation therapy are some examples [2, 4]. Common diagnosis procedures of prostate cancer include a Digital Rectal Examination (DRE), a palpatory examination of the prostate, and/or the measurement of the Prostate Specific Antigen (PSA). However, these methods are not definitive. DRE is effective for finding small tumors and

PSA changes can be non-cancer related, such as the enlargement of the prostate with age [16]. Currently, the most reliable diagnosis method is a core-needle biopsy under the guidance of transrectal ultrasound (TRUS) [9]. The biopsy involves taking tissue samples from predefined anatomical regions of the prostate, which means the procedure is performed blind. Conventional ultrasound imaging is not capable of differentiating cancerous and normal tissue regions with high sensitivity and specificity. New techniques have been proposed to enable a targeted biopsy by extracting tissue-type information from the ultrasound signal, in hopes of improving prostate cancer detection rate [12].

Machine Learning (ML) methods that use ultrasound data for prostate cancer detection utilize features extracted from radio frequency (RF) and B-mode ultrasound images are beginning to be utilized. Features from both B-mode images and calibrated spectrum of a single RF frame have been used to classify prostate cancer [5, 8, 20]. The major limitation of B-mode imaging is a loss of information due to post-processing of the signal, whereas analysis of single-RF-frame-spectrum suffers from the lack of a standard method of calibration [27]. Recently, a novel technique has been used for classification in a machine learning framework. A sequence of ultrasound RF frames is captured in time from a stationary tissue location (hereafter referred to as *RF time series* or *RFTS*) produces features for the machine learning [3, 11, 20, 21]. This RFTS method outperforms other ML techniques [21].

The project proposed by this report will investigate the physical mechanisms of the RFTS method, which was developed by our sponsor, Dr. Purang Abolmaesumi and his team [3, 11, 20, 21].

1.2 Project Objectives

While extensive studies have shown the effectiveness of classification using RFTS methods, less is known about why the variations even exist in the RF time series data . In the situation of RFTS, everything is held stationary in space. When taking ultrasound images from frame to frame, it is expected that the signal characteristics remain constant. However, this is not the case. The aim of the project is to connect physical meaning and investigate the sources of these time series variations. Hereafter the time series variations will be referred to as sources of *information*.

Previous work has identified three hypotheses (Table 1.1) that attempt to explain sources of information, which aid in the classification of tissue. Although the previous works have identified possible sources of information, their results are not decisive. More investigations must be carried out in order to come to a complete understanding. Furthermore, the end goal is to use this understanding, to then feed back into the RFTS method, in order to optimize it (choosing the

Hypothesis 1 [H1]:	Microvibrations in the tissue caused by acoustic radiation force and environmental factors, are captured by the RFTS as a source of information.
Hypothesis 2 [H2]:	Acoustic radiation force leads to increased tissue temperature, which differs among tissue types – seen by the RFTS as a source of information.
Hypothesis 3 [H3]:	Jitter (noise) in the transmitted signal affects the tissue response and is then captured by the RFTS as a source of information.

Table 1.1: This table shows the hypotheses determined from previous work. In this project, hypothesis 1, H1 will be tested and developed further. Hereafter, each hypothesis will be referred to as H1, H2, and H3 respectively.

proper features, designing the procedure in order to maximize prostate cancer detection, etc).

This project will be catered around answering one main set of research questions and it will serve as the sole objective of the project. We will mainly focus on one hypothesis, **H1**, dealing with microvibrations – the other two hypotheses will only be considered if time permits. So the questions will be answered in the context of **H1**:

Research Question(s):

What are the main sources of information which enable the RFTS method to be so effective and can they be described physically? If they can be described physically, what are the driving mechanisms and can we generate features from them? Can the mechanisms be taken advantage of and improve the RFTS method?

Project Plan:

In this project, we plan to do the following:

- Design ultrasound experiments that test the microvibration hypothesis (Table 1.1) using Phillips tissue phantoms, IU22 Ultrasound machine, and DAQ board.
- Simulate these ultrasound experiments with the software packages: Field-II, k-Wave, COMSOL/ANSYS.

The following section serves to provide ample background knowledge to critically think about and design experiments and interpret results.

1.3 Background

The use of ultrasound imaging has been greatly increasing for tissue typing in the past twenty years. *Tissue typing* is defined as an ensemble of techniques to compare and contrast structures between different types of tissue [22]. In order to conduct accurate tissue typing, it is imperative to understand the image formation and physical mechanism of ultrasound interaction with tissue. The relationship between ultrasound signals and tissue microstructure can provide information about the size and shape of aberrant tissue for diagnostic or treatment purposes.

The following section serves as an overview to prostate cancer and the diagnosis procedures using *conventional* ultrasound imaging, as this is the main application of the RFTS method.

1.3.1 Prostate Cancer

Prostate cancer is a malignancy that starts in the cells of the prostate. Being a malignant tumor, prostate cancer can spread, or metastasize, to other parts of the body. If diagnosed early, prostate cancer grows slowly and can be completely removed or managed successfully [wwww.cancer.ca].

Sometimes, changes in the cells of the prostate facilitate the conditions for cancer to grow. Cells may not be cancerous explicitly, but there is a higher chance these abnormal changes will become cancer. Precancerous conditions that can develop in the prostate are prostatic intraepithelial neoplasia (PIN), proliferative inflammatory atrophy (PIA) and atypical small acinar proliferation (ASAP) [wwww.cancer.ca].

1.3.1.1 Anatomy of Prostate

The prostate is part of the male reproductive system (Figure. 1.1). It is a walnut-sized gland just below the bladder and in front of the rectum. It surrounds part of the urethra, which is the tube that carries urine and semen through the penis. The prostate makes part a liquid called seminal fluid, which mixes with sperm from the testicles to make semen[wwww.cancer.ca].

1.3.1.2 Grading and Staging

Grading is a way of classifying prostate cancer cells based on their appearance and behavior when viewed under a microscope. The most common grading system is the Gleason classification system. The system is based on the structure of the prostate gland tissue. The Gleason system uses a scale between 1 to 5 (Table 1.2).[wwww.cancer.ca]

To assign a *Gleason Score* (also called the *Gleason Sum*), the pathologist looks at a biopsy sample of the tumor to find the 2 most common types of growth patterns. The grade given to both

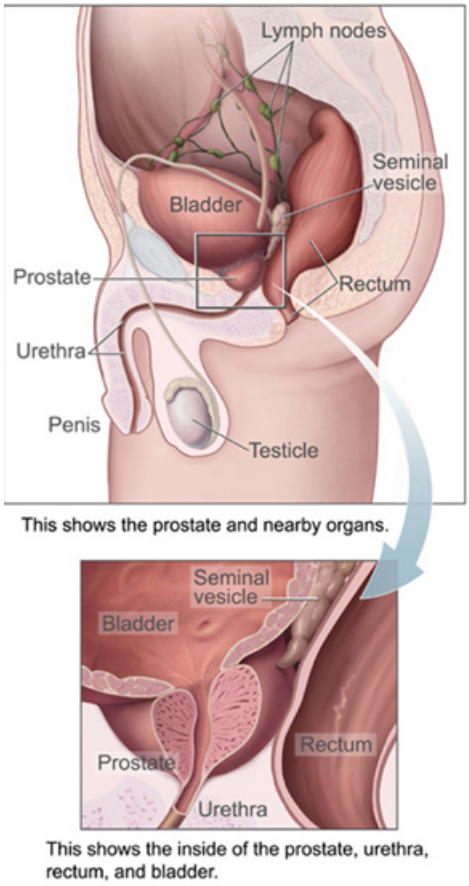

Figure 1.1: Prostate is an organ in the male reproductive system, just below the bladder and in front of the rectum. Courtesy of: https://commons.wikimedia.org/wiki/Category:Prostate#/media/File:Prostatelead.jpg.

Grade	Description
3	The cancer cells are well differentiated, which means they still form well-defined glands. The cancer has grown into, or invaded, the surrounding prostate tissue. The cancer is less aggressive and has a favourable prognosis.
4	The cancer cells are between grade 3 and grade 5.
5	The cancer cells are poorly differentiated, which means they are very abnormal and don't look and act like normal glands. The cancer is more aggressive and has a less favourable prognosis.

Table 1.2: This table shows the grading structure of the Gleason system. Grades 1 to 2 were omitted as the cancerous tissue shows negligible physical and behavioral differences with respect to normal prostate tissue – these indicate slow forming prostate cancer.

these patterns are summed to determine the score. Scores are always between 6 and 10 – higher scores indicate more aggressive tumors. Most prostate cancers are low to intermediate grades (6

to 7) [wwww.cancer.ca].

Staging is a way of describing or classifying the extent of cancer in the body (Table 1.3). The standard procedure to determine the stage of the cancer is to use the gleason score, biopsy, and PSA (prostate specific antigen) results. The most common staging system for prostate cancer is the TNM (tumor, nodes, metastasis) system. The TNM system assesses the extent of the primary tumor (T), presence of regional lymph node involvement (N), and distance metastasis (M) [10].

Stage	Description
I	Small and contained within the prostate.
II	Larger, but still within the prostate.
III	Beginning to spread outside the prostate.
VI	Completely has spread outside of the prostate.

Table 1.3: This table shows a summarized version of staging of prostate cancer.

1.3.1.3 Diagnosis

Early diagnosis, with accurate grading and staging of prostate cancer decreases the risk of mortality by facilitating proper clinical decision making. Decisions such as identifying the most suitable treatment options: surgery, radiation therapy, brachytherapy, thermal ablation, and cryotherapy [2, 15]. Proper grading and staging not only enables appropriate treatment options, but also reduces over-diagnosis [4, 28]. Over-diagnosis is when non-progressive and slow-growing cancer is diagnosed, resulting in unnecessary and harmful treatments [10]. Table 1.4 highlights several other diagnosis methods and some of their limitations. In the following report we focus on the RFTS ultrasound based technique and how to further understand the mechanisms that drive it, in order to improve prostate cancer detection.

1.3.2 Ultrasound Theory

1.3.2.1 Overview

The propagation of ultrasound through a medium can be approximated by the temperature independent, linear acoustic wave equation,

$$\frac{1}{\rho c^2}\frac{\partial^2 p}{\partial t^2} = \nabla \cdot (\frac{1}{\rho}\nabla p). \tag{1.1}$$

p is the pressure at a point in space and time, ρ is the density of the medium, and c is the speed of sound in the medium. Ultrasound interacts with tissue in four ways: reflection, refraction, scattering, and absorption, with absorption and scattering being the dominant mechanisms in a heterogeneous medium like tissue. The frequency used in medical ultrasound is upper-bounded by decreasing penetration depth and lower-bounded by decreasing resolution. Working frequency

Diagnosis Option	Description
PSA Measurement	PSA, prostate specific antigen, contributes in the current approach for diagnosis. There are limitations because factors, such as: prostate size, sexual activity, and aging, also elevate PSA levels [10] .
Digital Rectal Examination	DREs evaluate the stiffness of the cancerous tissue. DREs are usually combined with PSA measurements. This test is limited to superficial and large legions, since small tumors cannot be easily palpated in the prostate gland [14, 16].
TRUS Guided Biopsy	Trans-rectal ultrasound guided biopsies are the gold standard in today's diagonses. Procedure involves taking tissue samples from predefined regions. Shape, arrangement, and density as well as PSA levels are considered for diagnosis. The biopsy procedure is not scaled to individual patients, due to lack of sensitivity and specificity of TRUS. It has been reported that the Gleason Score achieved using biopsies, underestimates the score given by radical prostatectomy in 19% to 57%, and overestimates in 5% to 50% of cases [6, 7, 10, 23].
MRI	MRI and MRI+US combination approaches are also in use for diagnosing prostate cancer. Fusion of ultrasound and MRI has been used to improve prostate cancer detection by facilitating targeting of the cancer foci determined in the MRI during TRUS-guided biopsy [19]. These techniques require sophisticated mechanical systems to guide the biopsy needles. If performed by software only, patient motion or organ deformation is unaccounted.

Table 1.4: This table summarizes and describes the limitations of some of the current prostate cancer diagnosis techniques.

is usually between 6 to 10MHz. High frequencies in the 55MHz range have been used in some experiments, with reported improvements to classification accuracy.

1.3.2.2 Interaction with Tissue

As mentioned in the overview (Sec. 1.3.2.1), there are different ways that ultrasound can interact with tissue. Figure 1.2 outlines the different modes of interaction: attenuation, absorption, reflection, scattering, refraction and diffraction.

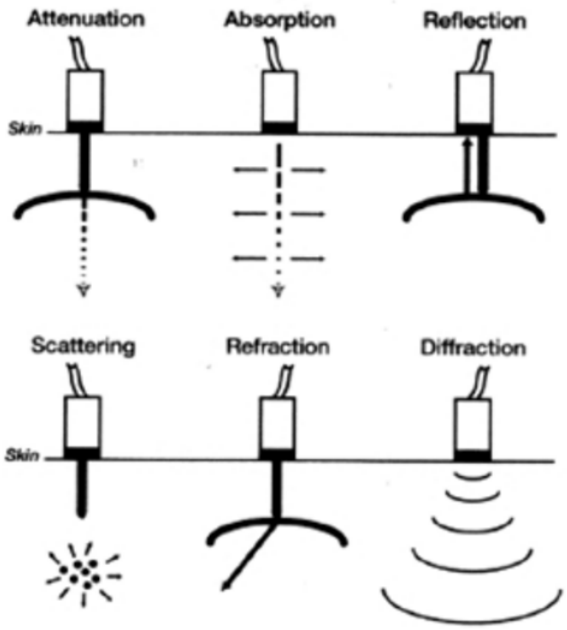

Figure 1.2: The different modes of interaction of ultrasound with tissue. Image courtesy of http://www.criticalecho.com/content/tutorial-1-basic-physics-ultrasound-and-doppler-phenomenon#.

Attentuation:

Attenuation is the term used to account for loss of amplitude (signal). In the context of this project, most of the attenuation is accounted by the remaining interaction modes: absorption, reflection, scattering, refraction, and diffraction. Because attenuation is a conglomerate of other phenomenon, its model is complex; it agrees well with experiments, but the theory cannot be formulated easily. Experiments suggest the amplitude decay model,

$$A(z) = A_0 e^{-\mu_A z}. \tag{1.2}$$

μ_A is called the amplitude attenuation factor and has units of inverse length. Since $20\log_{10}(\frac{A(z)}{A_0})$ is the amplitude drop in decibels, it is useful to define the attenuation coeffi-

cient α as,

$$\alpha = 20\log_{10}(\mathrm{e})\mu_A \approx 8.7\mu_A. \tag{1.3}$$

It is useful to think of α as a key parameter carrying all of the attenuation information. Often, the approximation $\alpha(f) \approx af$ is used in practice and so the following attenuation model results,

$$A(z,f) = A_0 \mathrm{e}^{-\alpha(f)z/8.7}. \tag{1.4}$$

Since the reflection time is a function of depth (z), one expects a weaker signal (stronger attenuation) as time progresses. This weaker signal is not necessarily less has reflected, but because there is less signal *to be* reflected. This time-dependent attenuation causes severe signal loss and image distortion, if not compensated. All ultrasound systems are equipped with Time Gain Compensation (TGC) circuitry – a time-varying amplification mechanism.

Absorption:

Absorption in soft tissue like skin, fat, tendons, ligaments, etc. accounts for 80% of ultrasound attenuation [http://usra.ca/tissue.php]. Absorption is the conversion of acoustic energy into thermal energy as the ultrasound waves propagate through the medium. Three main factors affect absorption: viscosity of the medium, relaxation time of the medium and the ultrasound frequency [25]. Increasing viscosity increases absorption. Relaxation time is proportional to the time taken by the medium particles to revert back to original mean positions following displacement by an ultrasound pulse. The longer the relaxation time of the medium, the higher the absorption [25]. Lastly, absorption increases with increasing frequency.

Reflection:

When a beam of ultrasound strikes the boundary between two mediums, it is partly transmitted and partly reflected. The reflected wave is called an echo and the production and detection of echoes form the basis of ultrasound. There are two types of reflection: specular and non-specular. Specular reflection occurs when the medium boundary is smooth and large relative to the beam. Non-specular reflection (also known as scattering) occurs when the boundary is irregular and small relative to the beam.

Reflection is considered specular when the diameter of the reflector is greater than the wavelength of the ultrasound beam. Models of specular reflection are simple,

$$\text{Specular reflection} \Leftrightarrow \text{Angle of incidence} = \text{Angle of reflection} \tag{1.5}$$

The amount of reflection that occurs at the boundary depends on the acoustic impedance of the two mediums,

$$Z = \rho v = \rho \frac{1}{\sqrt{\rho\kappa}} = \sqrt{\frac{\rho}{\kappa}}. \tag{1.6}$$

ρ is the density of the medium, v is the speed of sound in the medium, κ is the compressibility of the medium [25]. If the difference in acoustic impedance between the two mediums is small, a weak echo will be produced, and most of the ultrasound will carry on through the second medium. If the difference in acoustic impedance is large, a strong echo will be produced. This is seen in equation 1.7, which models the simple case where a beam strikes the reflector normal to its boundary.

$$\frac{I_{reflect}}{I_{incident}} = \frac{(Z_1 - Z_2)^2}{(Z_1 + Z_2)^2}. \tag{1.7}$$

$I_{incident}$ is the incident beam's intensity and $I_{reflect}$ is the reflected beam's intensity. Typically in soft tissues, the amplitude of an echo produced at a boundary is only a small percentage of the incident amplitudes [http://www.criticalecho.com/content/tutorial-1-basic-physics-ultrasound-and-doppler-phenomenon#].

Scattering:

Reflection is non-specular when the reflecting interface is irregular, and its size is small relative to the diameter of the ultrasound beam. Non-specular reflection (scattering) is difficult to model theoretically beause the incident beam is reflected in many different directions. This reflection is a function of the sizes of the scattering target and the ultrasound beam diameter. When the dimension of the structures on an interface becomes about one wavelength of the ultrasound beam, we enter the scattering regime. Typical wavelengths for diagnostic ultrasound beams is about 1mm. This is within the order of magnitude of micro-structures on an organ, hence making scattering a useful source of information for ultrasound imaging. Scattering shows very strong frequency dependence, increasing rapidly as the frequency of ultrasound is increased [25].

Refraction:

Refraction is a change in beam direction at a boundary between two mediums in which ultrasound travels at different velocities (V_1 and V_2). The change in velocity is caused by the change in wavelength as the ultrasound crosses from the first medium to the second while the frequency remains constant, The relationship between the angle of incidence and the angle of refraction is governed by Snell's law as in optics:

$$\frac{\sin(\theta_i)}{\sin(\theta_r)} = \frac{V_1}{V_2}. \tag{1.8}$$

Diffraction:

Diffraction of an ultrasound beam describes the spreading out of beam energy as it moves away from the source. Diffraction affects the intensity of the beam both axially and laterally. In diagnostic ultrasound, the dimensions of the ultrasound beam, and the manner in which it diffracts, has great influence on image resolution and imaging depths.

Diffraction determines the ultrasound beam shape. Typically, the ultrasound beam spreads out as it moves away from the transducer. In the *near field* regime or *Fresnel zone*, the beam is still narrow and has a diameter not much bigger than the piezoelectric crystal source. After a certain distance, the beam enters the *far field* regime, or *Fraunhofer zone* where it begins to diverge and diffract to a bigger diameter. This results in a degradation of spatial resolution of the image [26].

The **focus** of a transducer is the point on the central beam axis which is equidistant from all points on the surface of the transducer. For all linear paths between the focus and the surface of the transducer, the times of flight are equal. Areas within the beam close to the focus will have properties which will closely match those at the focus itself. This region around the focus is called the **focal zone** of the transducer. In the context of diagnostic ultrasound, it is ideal to have a well focused beam in the region of interest, in order to get an optimal quality image [26].

1.3.2.3 Imaging and Characteristics

The piezoelectric effect is the driving mechanism for ultrasound imaging. In piezoelectric materials, electrical charge is converted into a mechanical vibration and vice-versa. An ultrasound machine generates and transmits ultrasound beams to the target tissue through a set of piezoelectric crystals embedded within an ultrasound transducer [1]. The transducer both transforms electrical signals to an outgoing ultrasound beam and reconstructs an electrical signal from the returning echos [1].

An ultrasound machine focuses sound waves along a scan line, such that the waves constructively interfere at the desired focal point, as shown in Figure 1.3. As the sound waves propagate towards the focal point, they can reflect off obstacles they encounter along the propagation path. Once all of the returning waves have been collected by the transducers, new sound waves are transmitted towards a new focal point along the given scan line. Once the entire scan line has been measured by sound waves, the ultrasound system repeats the procedure along a new scan line until all of the scan lines in the desired region of interest have been measured [1].

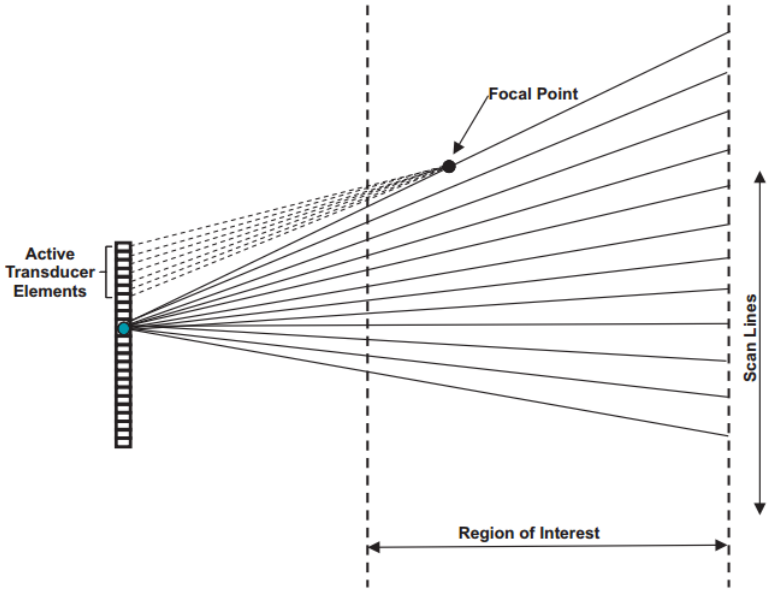

Figure 1.3: This figure shows the basic functionality of an ultrasound system. It demonstrates how transducers focus sound waves along scan lines in the region of interest. Image courtesy of [1].

To focus the sound waves towards a particular focal point, a set of transducer elements are energized with a set of time-delayed pulses to produce a set of sound waves that propagate through the region of interest (organ or tissue under examination). This process of using multiple sound waves to steer and focus a beam of sound is commonly referred to as beam-forming [1]. Post beam-formed data is referred to as radio-frequency (RF) ultrasound signals because the frequency range is similar to radio-frequency waves [10].

The quality of an ultrasound image determines its usefulness. The overall quality of the ultrasound image is not only dependent on the imaging system, but also from the performance of the operator. It is important to emphasize that the quality is the result of an optimization of many parameters. A discussion about image quality centers around image resolution. For an ultrasound image, the following types of resolution are relevant: spatial resolution, temporal resolution and contrast resolution.

Spatial Resolution:

Spatial resolution describes the ability to distinguish between objects located at different positions in space. It is the capability of the imaging system to depict structural detail. Spatial resolution is divided into two components: axial and lateral resolution. Axial resolution is the ability to distinguish between echos originating from reflectors lying one behind the other along the axis of the ultrasound beam. Lateral resolution is the ability to distinguish

between two reflectors side by side in a direction perpendicular to that of the ultrasound beam [24].

Axial Resolution:
Axial resolution can be defined with the following relation,

$$\text{Axial Resolution} = \frac{1}{2}\text{SPL}. \tag{1.9}$$

SPL is the spatial pulse length. The SPL is the distance at which the oscillations of an ultrasound pulse are damped completely. SPL is defined as,

$$\text{SPL} = \lambda \cdot \text{Number of cycles in 1 pulse}. \tag{1.10}$$

The axial resolution does not vary much with tissue depth, as does lateral resolution. Nevertheless, small variations do occur as a result of changes in the frequency spectrum of the beam. The frequency spectrum in the ultrasound beam is distributed around the center (intended) frequency. Because higher frequencies of ultrasound attenuate more quickly than lower frequencies, as the beam travels further and further, more and more of the beam will be low frequency components. The average wavelength increases, implying longer spatial pulse lengths and hence reduces axial resolution [24].

Lateral Resolution:
Typically in ultrasonic imaging, the axial resolution is greater than the lateral. This means that lateral resolution is the more limiting aspect of spatial resolution. Therefore it is important that the factors affecting lateral resolution be well understood [24]. These factors are:

- beam diameter
- beam frequency
- scan line density

Lateral resolution is limited by the beam diameter in the plane of the reflectors; reflectors closer to one another than the beam diameter cannot be resolved. Therefore, the smaller the beam diameter, the better the lateral resolution. In turn, the lateral resolution is dependent on tissue depth because the beam width may vary widely with distance along the beam path [24]. Frequency also affects lateral resolution by affecting the beam shape. The ultrasound beam is narrower at higher frequencies. Therefore, the higher the frequency, the better the lateral resolution. Also, the increased beam frequencies extend the near-field, although this advantage is partly counteracted by the increased attenuation at higher

frequencies.

The number of scan lines used to construct an ultrasound image also affects the lateral resolution. The image is formed by scanning the beam across the selected plane of interest in the object – therefore sampling the tissue at smaller intervals improves resolution. The higher the scan line density, the better the lateral resolution.

Contrast Resolution:

Contrast resolution is the ability to distinguish between signal magnitudes. In an ultrasound image, this means being able to differentiate between the intensities of the dots representing echoes of different intensity at the display. The ability to detect small changes in the characteristic echo pattern of an object may well depend on the contrast resolution. The electronics in the ultrasound system, and the inherent contrast properties of the display and recording devices affect the contrast resolution largely. The use of digital image processing techniques improves contrast resolution of ultrasound images [24].

Temporal resolution:

Temporal resolution is the separation of events in time and hence is important in real-time imaging. The rate at which image frames are generated and viewed affects the visualization of moving structures. In the context of ultrasound, one can control the temporal resolution by changing the system's frame collection rate, or f.p.s (frames per second). It is important to note that increasing f.p.s may present limitations due to the finite speed of sound (the distance traveled in one second that is required may be greater than the speed of sound in that medium) and can reduce lateral resolution by decreasing scan line density at a given tissue depth [24].

1.3.3 Time Series Analysis

The RFTS technique uses ultrasound time series data obtained from a stationary location of tissue, to characterize between various tissue types (Fig. 1.4). This approach has been effective at both high frequency (20–60 MHz) and clinical frequencies (2–10 MHz) [21]. After collecting the ultrasound data and some post-processing (envelope detection and log-compression), the data is sent to a Machine Learning framework – an SVM classifier. Within the framework, some features are constructed, such as: intercept and slope of the fitted regression line to the data, spectral properties, and fractal dimension. After the features are constructed, training, and validation occur before making classifications of other RFTS data.

The machine learning framework will be used heavily in this project. It will be used to quantitatively compare different experiments. The single, most important metric that will be

used is the classification accuracy – how well can the machine learning distinguish between tissues. We will test various scenarios, such as: how the feature value changes with respect to the experimental variable (microvibrations, temperature, jitter, or other), how the accuracy changes in different conditions, how does stiffness between tissue types play a role, and any other permutation we can conceive.

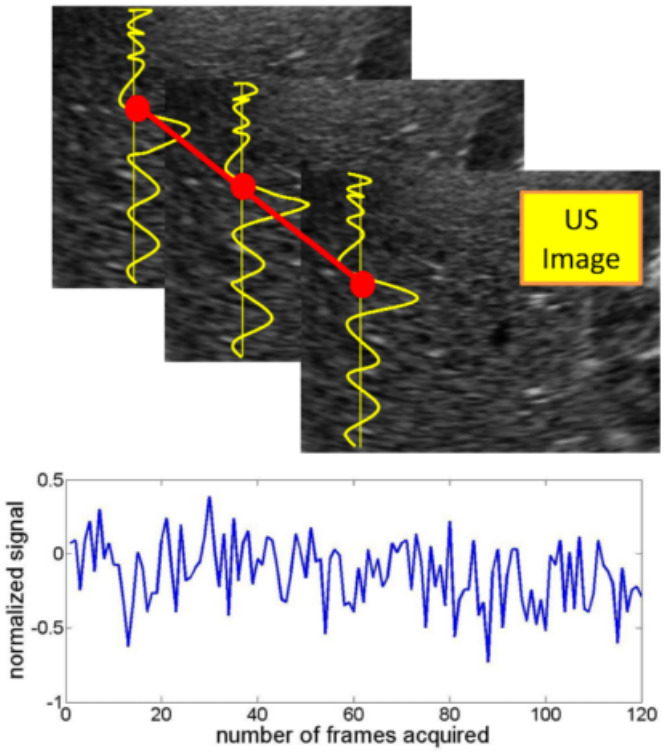

Figure 1.4: This figure shows how the RF time series signal is captured. The top part of the figure shows different frames of the same position being measured, whereas the bottom part shows the a sample data set plotted against time (frame number). Image courtesy of [10].

1.3.4 Bio-heat diffusion

The diffusion of heat is central to US dynamics and will be considered in both simulation and experiments. The diffusion of heat in tissue can be described by modeling the incident ultrasound waves as point heat sources, by using a simplified Pennes' bioheat equation,

$$\frac{\partial T}{\partial t} = \kappa \nabla^2 T + \frac{q_v}{c_v} \tag{1.11}$$

κ is thermal conductivity of the medium, q_v is the per volume heat influx from the ultrasound and c_v is the per volume specific heat capacity. Only a fraction of the incoming ultrasound is transformed into heat,

$$q_v = 2I\alpha(T)d \tag{1.12}$$

where I is the ultrasound intensity and α is the temperature dependent absorption coefficient.

1.3.5 Mechanical Properties: Healthy and Cancerous Tissue

We are motivated to investigate the effect microvibrations on ultrasound response of the medium by the fact that there are known mechanical differences between healthy and cancerous tissue.

1.3.5.1 Viscoelastic Theory

In order to understand these differences, we can model tissue as a viscoelastic material, one which shows both elastic and viscous mechanical behavior. A purely elastic material responds to an oscillatory stress (Eq. 1.13) linearly (Eq. 1.14) where $\epsilon(t)$ is the time-dependent strain. On the other hand, for a perfectly viscous material, the stress is related to the rate of change of the strain (Eq. 1.15). We note that a sine wave is a $\frac{\pi}{2}$ shifted cosine and that the viscous response is simply a phase-lagged variant of the elastic response.

$$\sigma(t) = \sigma_0 \cos \omega t \tag{1.13}$$

$$E(t) = \frac{\sigma}{\epsilon} = c \Rightarrow \epsilon(t) = \epsilon_0 \cos \omega t \tag{1.14}$$

$$\epsilon(t) = \epsilon_0 \sin(\omega t) = A \cos(\omega t - \frac{\pi}{2}) \tag{1.15}$$

A viscoelastic material will show some intermediate behavior between purely elastic and purely viscous. It will have a strain response of,

$$\epsilon(t) = A \cos(\omega t - \delta). \tag{1.16}$$

δ is a phase-lag between 0 (purely elastic) and $\frac{\pi}{2}$ (purely viscous). If the system is analyzed in the complex domain, one can define a complex Young's Modulus (Eq. 1.17) and corresponding elastic modulus (Eq. 1.18) and viscous modulus (Eq. 1.19):

$$E^* = \frac{\sigma^*}{\epsilon^*} = \frac{\sigma_0 \cos(\omega t) + i\sigma_0 \sin(\omega t)}{\epsilon_0 \cos(\omega t - \delta) + i\epsilon_0 \sin(\omega t - \delta)} = \frac{\sigma_0}{\epsilon_0} e^{i\delta}, \tag{1.17}$$

$$E_{elastic} = \mathrm{Re}[E^*] = \frac{\sigma_0}{\epsilon_0} \cos(\delta), \tag{1.18}$$

$$E_{viscous} = \mathrm{Im}[E^*] = \frac{\sigma_0}{\epsilon_0} \sin(\delta). \tag{1.19}$$

1.3.5.2 Mechanical Differences

Previous work using sonoelastography has shown significant differences in the viscoelastic properties between benign and cancer cells [29].

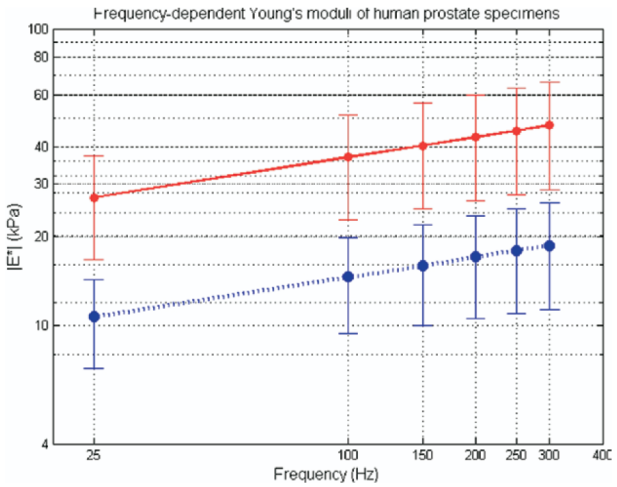

Figure 1.5: Plot of averaged magnitudes of complex Young's Moduli of normal (blue dotted curve) and cancerous (red solid curve) prostate tissue as a function of frequency. Standard deviations are also provided [29].

Figure 1.5 shows a difference in frequency-dependent resistance to mechanical stress. An incoming ultrasound wave is precisely an oscillatory mechanical stress and therefore should interact differently with healthy and cancerous cells. Furthermore, we hypothesis that microvibrations from the room affect the propagation of ultrasound waves inside the medium differently based on the viscoelastic properties of the medium. For example, a typical table fan operates at a frequency of 2000 rpm or about 33 Hz, well within the range of frequencies shown to elicit different strain responses between healthy and cancer cells (Figure 1.5). The response of the tissue to microvibrations then interferes with the incoming ultrasound wave. This hypothesis explains the result that when RFTS methods are used on a sample on an optical table, the classification is worse than an identical experiment where the sample is placed on a regular table. These results will be elaborated on in the previous-results section 1.4.1.

1.3.6 Simulation Tools

In this project we will simulate the physical experiments we will be conducting. These "simulation experiments" are to provide motivation to carry out the phantom (physical) experiments, provide preliminary results (order of magnitude effects of microvibration, etc.), and provide a way to compare experimental results and theory. There are two main software packages that we will use to create ultrasound simulations: *Field-II* and *k-Wave* [website links to both]. Additionally, we

will decide between two other software packages: *ANSYS* and *COMSOL*, to model microvibration in various media with various boundary conditions, acted upon by different types of sources. Some further detail about each software package is provided below.

1.3.6.1 Field-II

The Field program is a free-to-use MATLAB software package that performs ultrasound-tissue interaction simulations. It allows the user to define their own geometries, medium properties, and place scatterers anywhere within. Field does not provide simulations in time, but rather solves the incident, receiving, and signal model equations, at a given instant. Furthermore, Field also takes into account focusing and frequency dependent attenuation effects (uses a linear approximation) [13]. One of Field's limitations is that it does not take into account the change of sound speed due to thermal effects facilitated by acoustic radiation (whereas k-Wave can). How we will use Field-II in this project is elaborated in Chapter 2.

1.3.6.2 k-Wave

k-Wave is an open source MATLAB toolbox designed for the time-domain simulation of propagating acoustic waves in 1D, 2D, or 3D. The toolbox has a wide range of functionality, but at its heart is an advanced numerical model that can account for both linear and nonlinear wave propagation, an arbitrary distribution of heterogeneous material parameters, and power law acoustic absorption. k-Wave's role in this project is described in Chapter 2.

1.3.6.3 ANSYS and COMSOL Multiphysics

ANSYS Multiphysics and COMSOL Multiphysics are both FEA/Simulation software packages for various physics and engineering applications, especially coupled phenomena (multiphysics) [https://www.comsol.com/, http://www.ansys.com/]. In ANSYS, a full range of coupling options makes multiphysics simulation interactions – thermal-structure, thermal-electric, thermal-electric-structure, electromagnetic-structure, electromagnetic-thermal, electrostatic-structure, thermal-electric-fluid, fluid-thermal and fluid-structure – possible with ANSYS solutions. COMSOL is able to do similar types of simulation, as ANSYS and COMSOL are competing software.

In this project, we have access to both COMSOL and ANSYS – and we are particularly interested in vibrations studies. For efficiency, it is desirable to only work with one of these types of software. Both ANSYS and COMSOL have user-friendly interface options. For example, ANSYS Workbench is a streamlined version of ANSYS whereby the user can easily create geometries and perform simulations. On the other hand, COMSOL has a MATLAB API, which allows the user to

utilize the full power of MATLAB and its toolboxes in preprocessing, model manipulation, and postprocessing. The final decision on which software to use will be made by January 4, 2016.

1.4 Previous Results

The following section describes the previous work targeting the 3 hypotheses (Table 1.1). After a brief summary of the investigations, their conclusions are discussed.

1.4.1 Microvibration Studies [H1]

A previous study on the microvibration hypothesis showed that tissue classification performs worse in the absence of vibration sources in the environment. The RFTS method was used to classify different phantoms (varying scatterer sizes and elasticities), first on a regular table, then on an *optical* table, where external vibration is minimized (see Table 1.5) (under constant ultrasound settings).

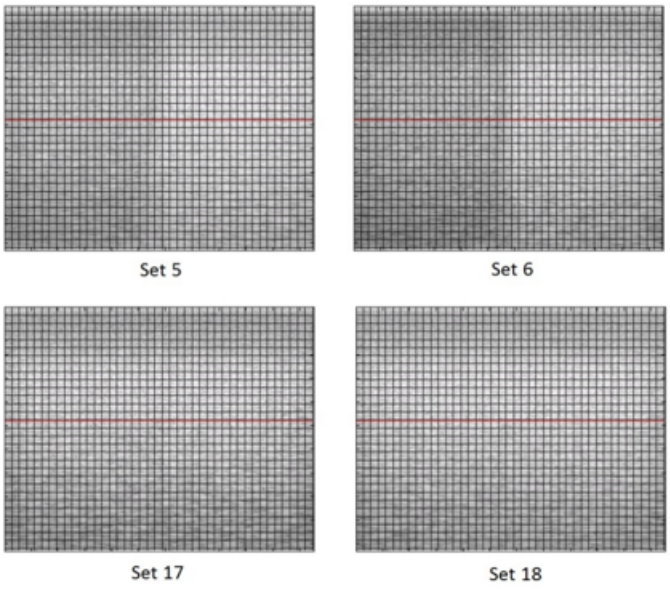

Figure 1.6: This figure shows the post-processed (applied Hilbert transform, then log-compressed) B-mode ultrasound images of four different phantoms. If we consider an arbitrary set, the left and the right side have different properties (Table 1.5). The machine learning takes each half and divides it into two sets, the training set and the testing set. Results are the performance of the trained classifier on the testing set, summarized in Table 1.6.

The results shown in Table 1.6 show that both the classification accuracy and discrimination power are much greater when the image is not taken on an optical table. Hence, we infer that

tissue vibrations caused by acoustic effects and the environment around the setup changes the backscattering of ultrasound, in the favor of enhanced classification. Experiments dealing with the investigation of this effect will be carried out – details of such experiments can be found in Section 2.2.

Experiments				
	Set 5	Set6	Set 17	Set 18
Phantom	Scatterer		Uniform Elasticity	
Description	Left: 30-50 micron		Left: 34 kPa	
	Right: 7-10 micron		Right: 15.9 kPa	
Table	Optical	Regular	Optical	Regular

Table 1.5: This table shows the description of each situation in the previous microvibration experiment. Each set corresponds to the B-mode images in Figure 1.6. For each set, the phantom consists of two physically different properties (left and right – corresponds to left and right in the figure) and the machine learning is meant to classify the left and right side.

Results				
	Set 5	Set6	Set 17	Set 18
Classification Accuracy	78%	98%	54%	94%
AUC	0.82	1.00	0.48	0.98
Table	Optical	Regular	Optical	Regular

Table 1.6: This table shows the results from the machine learning.

The study concluded that there must be further investigation into this effect – and to give possible explanations on why microvibrations of the surroundings enhance the classification power. One of the goals of this project is to attempt to explain this microvibration enhancement phenomenon.

1.4.2 Temperature Studies [H2]

Previous studies on the hypothesis of temperature rise associated with the effectiveness of classification are based on the idea that the speed of sound inside a tissue changes with increasing temperature [3]. The temperature dependence of speed of sound is characteristic of different tissue.

Daoud et al. were able to show a temperature dependence in time and power spectrum density (PSD) shifts of the ultrasound response [3]. Furthermore, they showed that features extracted from time and PSD shifts can be used to classify chicken and bovine tissue. However, the features used by Daoud et al. do not perform as well as state-of-the-art ultrasound classification features [3]. Hence, we infer that the time and PSD shifts caused by temperature increase do not

adequately explain the success of ultrasound classification.

Daoud et al. exaggerated the temperature increase in their study by using a 500 fps ultrasound source. This project can expand on the study by investigating settings closer to clinical settings, for example by reducing the frame rate to 20 fps Section 2.3.

1.4.3 Jitter Studies [H3]

Finally, preliminary studies have been conducted on the effect of jittering on classification accuracy. In a study, numerical simulation was used to predict the ultrasound response of tissue to a jittering ultrasound source (variable fluctuation in amplitude, phase shift, offset). The results of the simulation were then sent to the machine learning framework. Finally to compare all of the simulations, ROC curves were generated. While the results were inconclusive, small changes in amount of jitter changed ROC curve scores by upwards of 10%. This justifies the need for more experiments to investigate the jitter hypothesis. We will design experiments testing this hypothesis if time permits.

CHAPTER 2

PROPOSED SOLUTIONS

This chapter will discuss the main types of experimentation we will conduct. Our experimentation will be two-fold: Simulation and Phantom Studies. The goal is to try to conduct the same experiment in both modes, so that the results can be meaningfully compared. It is important to note that for each of the non-preliminary studies, we will repeat the experiment many times with different ultrasound parameters. These parameters include (but not limited to): center frequency, fps, imaging depth, focal depth, and wait time.

2.1 Preliminary Studies

The purpose of these experiments are to familiarize ourselves with the software and ultrasound machines.

2.1.1 Familiarization with Ultrasound Technology

2.1.1.1 Motivation

To understand and learn how to use the Phillips phantom ultrasound machines and the post-processing required to interpret data.

2.1.1.2 Proposed experiment

3D print simple structures like a spheres or cubes and use the ultrasound machine to determine the shape of these objects and their hollow features inside.

2.1.1.3 Simulation

Use k-Wave and Field-II to simulation the US images of the situation.

2.1.1.4 Materials

A Phillips IU22 phantom ultrasound machine will be used, along with 3D printers and a small amount of ABS/PLA plastic. The objects will be designed in SOLIDWORKS.

2.1.1.5 Analysis

Post-processing of the US data from the experiment and simulation will be analyzed in MATLAB to determine the structure of the sample object.

2.1.1.6 Verification

The results of the analysis will be verified with the sample object.

2.2 Microvibration Studies

Microvibration is the primary focus of this project. The following section outlines the experiments we are proposing to the sponsors.

2.2.1 Optical Table

2.2.1.1 Motivation

As discussed in the section 1.4, data exists to suggest that classification is worse on an optical table than a regular table. However these results are inconclusive. We will expand on previous studies and further investigate the effect of reducing or augmenting vibration on classification accuracy.

2.2.1.2 Proposed experiment

We will collect US data while varying the amount of "natural vibration noise," (noise from devices typically found in a lab). That is, we will conduct experiments with the the medium on an optical table, on a regular table, or on a table with added noise. The added noise will come from placing fans and other vibrating lab equipment in the vicinity of the experiment table.

2.2.1.3 Simulation

To conduct the simulation in this case, multiple software packages must be coupled. Since we do not want to include thermal effects, Field-II will be used to simulate the US image. First we create the geometry of the situation, then in Field-II we define scatterer locations. Within

ANSYS/COMSOL we much create the same geometry and location of scatterer, then simulate the effect of the microvibration source to get the axial displacement of the scatterers at each time step. At the corresponding time steps, we use Field-II and add in the axial displacement (change position of scatterers) to simulate the B-mode image. By the end of it we will get have obtained simulated RFTS data.

2.2.1.4 Materials

The same materials as the previously mentioned experiments. Optical tables are available in the laboratory.

2.2.1.5 Analysis

We hope to verify the relationship between the amount of vibration noise from the room and classification accuracy. As previous experiments have suggested, we should see lower classification accuracy in experiments on optical tables and possibly higher classification accuracy in experiments with added noise.

2.2.1.6 Verification

The SVN classifier will be used to compare classification accuracy between different experimental setups. Additionally, we will analyze which classification features changed the most between setups and reason about how vibrations are affecting the US data. These conclusions will serve as guides to designing future experiments.

2.2.2 Classification Accuracy with Controlled Mechanical Vibrations

2.2.2.1 Motivation

We saw in the background section (Sec. 1.3) that there are differences in density and viscoelastic properties between healthy and cancerous cells. These differences can cause different response to vibrations which will in turn affect the propagation of ultrasound through the medium. Past experiments that compared set-ups on optical tables versus regular tables showed that optical tables worsened classification. We infer that vibrations create the differences in features between healthy and cancer cells.

2.2.2.2 Proposed experiment

We will construct an apparatus that varies the intensity of the mechanical vibration. For the same vibration intensity, we will place different mediums on the platform and collect US data. We then see if classification improves or worsens. The induced vibrations should be periodic.

Noise in a clinical setting such as vibrations of a patient's cardiovascular system, breathing, etc. are regular.

2.2.2.3 Simulation

To conduct the simulation in this case, multiple software packages must be coupled. Since we do not want to include thermal effects, Field-II will be used to simulate the US image. First we create the geometry of the situation, then in Field-II we define scatterer locations. Within ANSYS/COMSOL we much create the same geometry and location of scatterer, then simulate the effect of the microvibration source to get the axial displacement of the scatterers at each time step. At the corresponding time steps, we use Field-II and add in the axial displacement (change position of scatterers) to simulate the B-mode image. By the end of it we will get have obtained simulated RFTS data.

2.2.2.4 Materials

We will build a frequency-controlled vibration apparatus using a loud speaker and signal generator. The sponsors have advised us to borrow the speaker from a neighboring lab and offered to purchase additional equipment.

2.2.2.5 Analysis

We are testing our hypothesis that vibration in the medium will affect the propagation of US in the medium and that different mediums will affect the US in distinguishable ways. The numerical simulations will predict whether vibrations in the medium are strong enough to affect the propagation of US and if so, under what conditions the vibrations will affect the propagation of US (threshold amplitude, frequency, etc.). Hence, the simulations may be a guide to deciding the areas of parameters space we want to investigate. Experimental results will be compared to numerical simulations.

2.2.2.6 Verification

A positive result for our hypothesis is a noticeable trend in how US features are changing with varying frequency and amplitude of the induced-vibration. This relationship of feature to frequency (or amplitude) of induced-vibration will differ based on the viscoelastic properties of the mediums. The features themselves can be analyzed and plotted against frequency (or amplitude). However, as final verification, we will classify different mediums using differing vibration settings. If our hypothesis is correct, the classification accuracy should be statistically different under different vibration settings.

2.3 Temperature Studies

The following section highlights possible experiments to be done, studying the thermal effects in the RFTS technique. These experiments will only be conducted if time permits – we give priority to the microvibration studies.

2.3.1 Tissue Classification Accuracy of Ultrasound-Induced Temperature Changes in a Clinical Setting

2.3.1.1 Motivation

Ultrasound RF locally increases the temperature of tissue during a time series scanning procedure. The rate at which the temperature rises is dependent on the composition of the tissue. Previous experiments have been able to show that tissue sound speed can be used to differentiate between water-based and lipid-based tissues, which respectively increase and decrease acoustic propagation speed as temperature increases.

2.3.2 Proposed experiment

Develop a temperature controlled environment to consistently generate a uniform sample temperature and collect US data at a frame rate of 20 fps. To simulate a patient's body, the temperature of the tissue sample should be tested at around 37 degrees Celsius, the internal body temperature of an average person. The time and PSD shifts in the US response will be tested with various tissue samples to determine whether the experimental results of Daoud et al. can be reproduced in a clinical environment.

2.3.2.1 Simulation

To conduct the simulation in this case, we only need to use k-Wave because we want include thermal effects. Our project sponsor has some scripts that solves the Pennes bioheat equation (Eq. 1.12), which will also help us determine the steady-state solution of the system.

2.3.3 Materials

The sample and apparatus would be placed in a temperature controlled water bath or enclosed chamber that we will design and construct. Other options would be to use an existing system such as a modified sous-vide machine or other apparatus available on campus.

2.3.3.1 Design

There will be a hard plastic spacer between the ultrasonic probe and the sample to reduce the effect of heat created by the piezoelectric components, and a layer of tissue-like material

underneath the sample to minimize the acoustic reflection off the back surface of the sample. This complete assembly will then be placed inside the temperature controlled environment.

2.3.3.2 Analysis

Results will be compared to those of previous publications. In particular, the classification accuracy of different tissue samples will be investigated to determine the merit of this experiment in a clinical setting. Data will also be collected at various incremental temperatures to isolate the temperature dependent features of the US response.

2.3.3.3 Verification

Similar classification accuracy as in previous published experiments.

2.4 Deliverables

Because this is a research project, there is uncertainty with what we can present as the final product. For the simulations, there are issues with intellectual property rights as the sponsor may not want to make the code public. Upon discussion with the sponsor, we will aim to produce an academic paper for publish but whether we achieve this goal is contingent on experimental results. Nevertheless, we will at minimal produce a report with all the simulations, experiments conducted as well as our analysis of the results. Specifically, we will outline the rationale for conducting the experiments we did (which may be different from the rationale outlined in this report as experimental results change our plan), the instruments and experimental setups we assembled and details of our software system (even if no code is included).
To summarize, here are a list of possible deliverables:

- Academic Paper.
- The Field-II, k-Wave and COMSOL/ANSYS scripts.
- Report of experimental results.

CHAPTER 3

PROJECT PLAN

This chapter will summarize logistical aspects of the project. A discussion about team responsibilities, project timeline, equipment, budget, location of work and issues of safety will be discussed.

3.1 Team Responsibilities and Contacts

Project manager: Conrad Ng

- Ensures that the schedule is maintained and work is done according to schedule.
- Maintains communications with the client and resource people.
- Schedules meetings and resolves general problems that arise.

Editorial manager: Kevin Multani

- Submits the Proposal and the Recommendation Report.
- Delegates the preparation of these documents.
- Ensures weekly reports are submitted to the project advisors.
- Records alterations to the schedule and milestones.

Technical manager: Kevin Shen

- Obtains access to equipment and resources.
- Maintains drawings, calculations, and software for the project.
- Sets up experiments and collects data with assistance from other team members.

With respect to general project responsibilities and roles, we will have Kevin Shen and Conrad Ng spearheading the simulation, and phantom experiments, respectively. Kevin Multani will work together with Conrad and Kevin S., on their respective duties and help integrate the two different sides of the project. More detail can be found in the Gantt chart (Figure 3.1) and in Section 3.2.

Technical Contacts:

1. Dr. Purang Abolmaesumi: Project sponsor.
2. Farhad Imani: Post-doc working in the project, he will be main contact in the day to day work.
3. Darrick Lee: Past ENPH459 student and has some experience with ultrasound technology – can tell us what to expect from a student's point of view.
4. Ben Macleod: Engineering Physics alumni, he is a Master's student currently at UBC working with the LAIR (Laboratory for Atomic Imaging Research). His thesis focuses on understanding and optimizing the performance of the LAIR,Äôs ultra-low vibration facility by studying how vibrations propagate from the earth through the isolation system and experiment structures to the tunneling junctions of our various microscopes, as well as the influence of acoustic fields. Great source of microvibration help.
5. Laurent Pellisier: Expert in ultrasound, CEO/CTO of Ultrasonix.
6. Tim Salcudean: Professor at UBC, expert in Elastography and US imaging. His current project is: Identification of tissue parameters using ultrasound vibro-elastography.

3.2 Work Plan and Project Schedule

Below is a rough work plan (in chronological order) to be started January 4, 2016, for complete timeline information please see the Gantt chart, Figure 3.1. There are a few things we will complete before January 4: gain access to the lab, install and run 'hello world' example code, the various software needed, more background reading on related topics, and see the new phantoms and DAQ board (sent by Phillips Research North America).

1.

Kevin M. and Kevin S. begin work on simulation the simulation. Kevin M. works with FEM software (ANSYS or COMSOL) to generate data that simulate vibration of a medium (different elasticity, density, scatter sizes). Kevin S. works on ultrasound simulation using Field II and k-Wave packages.

2.

Simultaneously, Conrad Ng and Kevin M. will work towards interfacing the new Phillips DAQ, writing the source code and protocols for opening data, saving data to hard disk, etc. and then will work on data acquisition code. Essentially, prepare the DAQ ready to use for phantom experiments.

3.

After Conrad Ng and Kevin M. are finished the interfacing, they must work with Kevin S. to generate an excel spreadsheet elaborating the amount of phantom experiments (what parameters to change from experiment to experiment, etc.). This spreadsheet must be approved by the sponsor.

4.

Conrad Ng and Kevin M. will begin conducting experimentation and collecting data. By now, the simulation codes are done – should try to emulate the 'real' settings in the code.

5.

When all the experimentation/simulation is complete all three persons will conduct data analysis – work towards a final report / publication.

6.

If time is left over – conduct other experiments regarding thermal effects / jitter (the other two hypotheses).

It is important to note that in our Gantt chart, we did not explicitly allot times for midterms and exams for other courses, but we considered the delay they might entail.

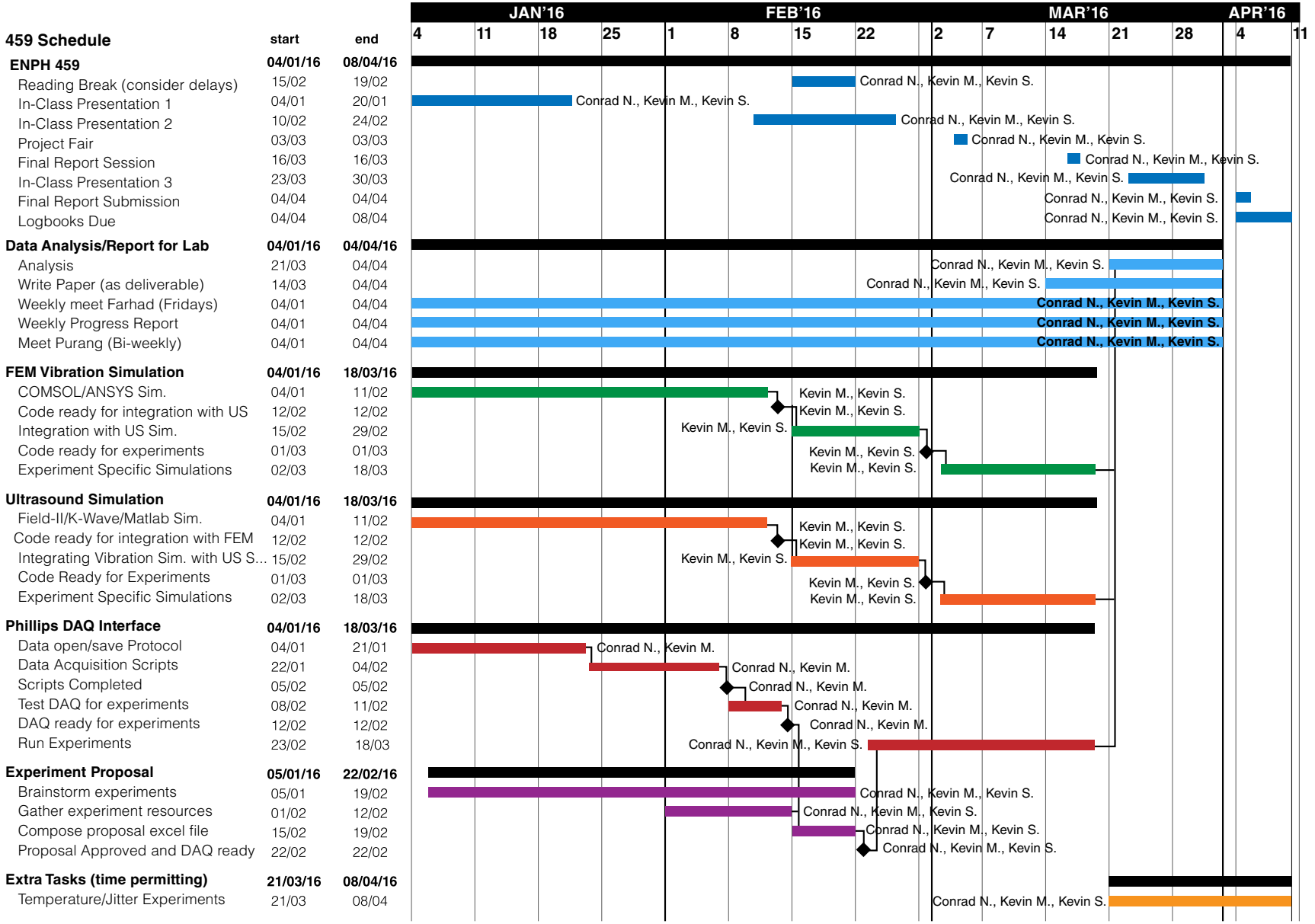

Figure 3.1: This is the gantt chart for this project.

3.3 Milestones

Risks associated with each milestone will be addressed in the contingency plan section.

1. Milestone: DAQ-CPU interface complete
    - Expected Date: Feb. 12
    - Weight: 35%
    - What will be accomplished: Finished scripts to interface the DAQ board. This includes scripts to open and save files from the DAQ as well as scripts for data acquisition. The DAQ should be ready and tested for experimentation.
    - What tasks we will begin: We can begin writing our experimental proposal, gathering resources for the experiments and setting up microvibration-experiments.
2. Milestone: Experimental proposal (excel sheet) approved by sponsors
    - Expected Date: Feb. 22
    - Weight: 30%
    - What will be accomplished: Experiments approved and the required resources to carry out the experiments have been gathered.
    - What tasks we will begin: We will begin experimentation.
3. Milestone: Simulation code ready to simulate experiments
    - Expected Date: March 2
    - Weight: 35%
    - What will be accomplished: FEM simulation integrated with US simulation, code is capable of simulating experiments we thought up in the proposal.
    - What tasks we will begin: Begin simulation relevant to the experiments.

3.4 Safety Plan

The scope of the project does not involve many hazardous items, if any at all. Ultrasonography is generally regarded as a safe form of imaging (Ultrasound safety: What are the issues?). We will adhere to any safety protocol that is applicable to the lab: electrical, fire, chemical – and read the corresponding manual, or follow guidelines provided by Dr. Abolmaesumi and his team. Otherwise, we have confirmed with the ECE department that no additional safety training is necessary.

3.5 Communication Plan

The sponsors have agreed to the following communication schedules:

- Meeting with Dr. Purang Abolmaesumi every 2-3 weeks.
- Weekly meetings with Dr. Farhad Imani.
- Submitting weekly reports to Dr. Farhad Imani, Dr. Purang Abolmaesumi.

Specifics dates for the meetings have not been set because the sponsors encouraged meetings based on necessity rather than a set schedule.

3.6 Location of Work and Budget

All, if not, most of the work will be conducted in the Kaiser building at UBC, room 3080–3090. We will unlimited lab access started January 4, 2016 (as long as the building is open). All of the equipment and resources are in the lab already – except the new DAQ board and new phantoms. The new material will arrive before we start in January. Ultrasound machine time is organized by a sign-up sheet, as other students/projects are also using the same machines we are. There are two types of ultrasound machines available for us to use: Ultrasonix, and Phillips (see Sec. 3.7). We will mainly be using the Phillips machine as the new DAQ board can only be interfaced with it.

3.7 Equipment

This section outlines equipment we will be using throughout the project. For experiment-specific equipment, refer to the experiment section 2.1.

3.7.1 Ultrasound Machines

3.7.1.1 Analogic SonixTouch Ultrasound System

System Overview

The SonixTouch Ultrasound system is a diagnostic ultrasound system that is able to perform a variety of imaging modes, ranging from the standard B (brightness) mode where display brightness is used to indicate amplitude, to the Colour/Power Doppler mode that superimposes a colour map onto the B mode to illustrate blood flow [18].

System Components

This ultrasound system consists of a LCD display, touch screen on an operator console, side connectivity panel for data transfer (USB ports), and a system case capable with three transducer

ports. The entire assembly is mounted on a wheelbase with four casters and has front/back handles for high mobility.

Imaging Modes

The SonixTouch is capable of performing B-mode, M-mode, Continuous Wave (CW) Doppler, Pulse Wave (PW) Doppler, Colour/Power Doppler and 3D imaging modes. Documentation for each of these modes can be found in [1].

Data Post-Processing and Output

The system is equipped with the data acquisition and software to perform the necessary front, mid and back-end processing to export image files in a .pdf format. The DICOM data files can also be transferred to a USB for other advanced post-processing.

3.7.1.2 Philips iU22 Ultrasound System

System Overview

The Philips iU22 Ultrasound System is a mobile diagnostic ultrasound unit designed to acquire, process, and display ultrasound data. The system has a wide range of imaging modes and can be used in various applications such as abdominal, musculoskeletal, pediatric, and prostate imaging.

System Components

This Philips ultrasound machine, with its power supplies, signal/image processing motherboards, four transducer acquisition slots, read/write DVD unit, and control panel with a video monitor, rests on a rolling frame with four swivel casters. The system has a fully integrated user interface capable of accessing all of the software features described in [17].

Imaging Modes

The iU22 is equipped with the capability of B-mode, M-mode, Continuous Wave (CW) Doppler, Pulse Wave (PW) Doppler, Colour Power Angio (CPA), and 3D imaging modes.

Data Post-Processing and Output

The ultrasound system can handle up to 1,024 scan lines at 500 frames per second depending on the transducer and mode. Post-processed full frame .JPEG images and DICOM files can be copied to DVD's for further analysis

Figure 3.2: Analogic SonixTouch Ultrasonix picture obtained from http://www.ultrasonix.com/webfm_send/1121

Figure 3.3: Phillips IU22 picture obtained from http://www.healthcare.philips.com/main/products/ultrasound/systems/iu22/

3.7.2 Probes

Transducer probes rely on the electro-mechanical properties of piezo-electric elements to generate sound waves and measure the reflection. During transmission, high voltage pulses traveling through the piezo-electric components produce sound waves that travel through sample tissue. During reception, miniature displacements in the elements generate small voltage waveforms. Transducers are generally expensive due to the delicate impedance matching required at the probe-skin boundary to minimize reflection.

A typical ultrasonic transducer consists of a piezo-ceramic element located between a ground and signal electrode. The electrodes are connected to signal wires which are soldered to a cable bundle and standardized connector (Fig. 3.4). An acoustic absorber is fixed to the back of the signal electrode to reduce interference from external sound waves traveling down the probe. The other side of the piezo-ceramic element points towards the tissue of interest, so multiple stages of varying acoustical impedance are layered on the probe tip. These layers are typically glued and then machined to finely control thickness, and expensive and time-consuming procedure. An acoustic lens is added to help focus the sound waves.

Analogic SonixTouch Ultrasound System

The transducer used with the Analogic SonixTouch System is the L14-5/38 Linear transducer. It has a frequency range of 5-14 MHz, and a focal range of 2-9 cm. This transducer is used for imaging smaller parts of the body with high resolution but relatively shallow depth. In linear probes like this L14-5/38, the piezo-electric elements are aligned in a linear fashion, resulting in

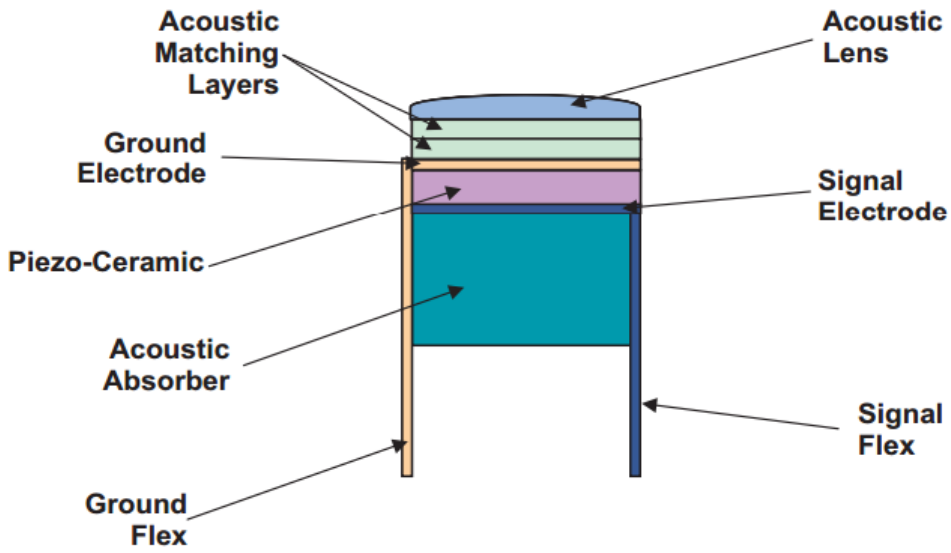

Figure 3.4: This figure shows a detailed cross-section view of an ultrasound transducer. Image courtesy of [1].

rectangular ultrasound images.

3.7.3 Phantoms

New Phillips phantoms are currently being shipped to the laboratory. No specifications will be given until the shipment arrives. However, These phantoms will have different elastic properties and scatterer sizes.

3.7.4 DAQ Board

Philips has developed a data acquisition board for their ultrasound systems. Only three of these DAQ boards and ultrasound systems have been made; one for Philips Healthcare facilities, one for the National Institute of Health (NIH), and one for Dr. Purang Abolmaesumi and his laboratory at UBC. Very little documentation exists for these boards, and we expect to spend some time learning how to interface these boards with the ultrasound machines.

3.8 Risks Anticipated and Contingency Plan

Below is a table of all the anticipated risks and the corresponding contingency plan (Table 3.1). As this is more of a research based project, most of the risks are ones that can't foresee – the unknown unknowns. We have tabulated most of the main things that could go wrong, and will respond accordingly.

Risk Condition	Probability of Occurence	Impact to project -/10	Action	Date of Action
FEM or US simulation is very difficult or impossible in the soft platform we choose. We will be choosing between COMSOL/ANSYS to model vibrations and, Field-II/K-wave/MATLAB to model ultrasound. Certain features may turn out to be very difficult to model using a certain platform, for example, lattice vibrations in phantom.	20% We need to go into the source code to do most of the changes for the simulations.	10	If one software platform imposes too many roadblocks, we will need to switch to another, but switching between platforms will cost a lot of time.	February 11th: We should know as soon as possible which platform most suits our needs.
Phillips IU22 machine DAQ Board cannot be interfaced to computer for data acquisition.	10-25% The DAQ board is custom-made (only 3 have been built) which means it may be difficult to use and troubleshoot (need to contact Phillips directly).	8	We will proceed with the Ultrasonix Analogic SonixTouch machine instead. The sponsor has said this machine is noisier.	January 25th: We should identify this problem before we propose experiments, but we can't identify it until someone has spent sufficient time trying to use the DAQ board.
Ultrasound machines not available (broken, in-use, etc.)	5% There are multiple machines in the lab and we can book the machines well ahead of time to mitigate the risk of machines all being used.	8	We proceed with other tasks (simulations, phantom experiment design, etc.) while waiting for ultrasound machines to become available.	February 23rd: We need to know before starting any experiments.
Experimental equipment not available. For example, we are expecting to borrow the speakers for our controlled-vibration setup from the elastography research group at UBC.	10% This should not happen because we will make sure to ask groups ahead of time whether we can borrow equipment and order equipment ahead of time.	7	We will try to purchase equipment if we cannot borrow them. If we cannot get the required equipment, then our experiments will be limited.	February 15th: We should know what equipment we will have, before submitting the experiment proposal to the sponsors.
Not getting phantoms on time.	10-30% Some phantoms have already been ordered and will come in soon.	7	If the phantoms have not come in by the time we started experiments, we would need to change the schedule of the experiments.	February 15th: We should know what phantoms we will have, before submitting the experiment proposal to the sponsors.

Table 3.1: This table outlines the risk conditions and corresponding contingencies.

CHAPTER 4

DENOUEMENT

4.1 Conclusion

The goal of this project is to investigate the sources of information that make the RFTS technique so effective. To meet this end, three hypotheses have been procured from previous studies. The project will focus mainly on hypothesis **H1** which states that microvibrations caused by the US probe, and by the environment enhance the RFTS techniques' classification power. To investigate hypothesis **H1**, studies have been designed consisting of a combination of simulations and phantom experiments. The simulations involve working with the MATLAB packages: Field-II and k-Wave, and the commercial FEM software: ANSYS and COMSOL. In the next 4 months we will accrue data to test this hypothesis, and if time permits, test thermal and jitter effects (**H2** and **H3**, respectively). We have full-access to the laboratory starting January 4, 2016. Phantoms specifically designed for this study will be arriving in the next few weeks, as well as a new DAQ board – both of which were designed by Phillips Research North America.

4.2 Timeline Overview of Proposal

4.2.1 Proposal One

Sept. 25, 2015 Constructed all major sections of the proposal.

Oct. 8, 2015 Started to fill out background sections: prostate cancer and machine learning.

Oct. 19, 2015 Hand in first proposal.

4.2.2 Proposal Two

Nov. 8, 2015 Added major sections on ultrasound theory and previous experimental results.

Nov. 9, 2015 Handed in second proposal.

4.2.3 Proposal Three

Dec. 2, 2015 Realize that we don't know what we are doing.

Dec. 4, 2015 Determined what we need to do – complete overhaul of sections.

Dec. 10, 2015 Added chapter 2, chapter 3.

Dec. 14, 2015 Filled in background sections, previous work, inputted gantt chart, risk assessment table.

Dec. 16, 2015 Made final revisions to proposal, wrote executive summary, letters of transmittal, and conclusion.

BIBLIOGRAPHY

[1] M. ALI, D. MAGEE, AND U. DASGUPTA, *Signal processing overview of ultrasound systems for medical imaging*, SPRAB12, Texas . . . , (2008), pp. 1–27.

[2] R. CHOU, J. M. CROSWELL, T. DANA, C. BOUGATSOS, I. BLAZINA, AND R. FU, *Review Annals of Internal Medicine Screening for Prostate Cancer : A Review of the Evidence for the*, Ann Intern Med, 155 (2011), pp. 762–771.

[3] M. I. DAOUD, P. MOUSAVI, F. IMANI, R. ROHLING, AND P. ABOLMAESUMI, *Tissue classification using ultrasound-induced variations in acoustic backscattering features.*, IEEE transactions on bio-medical engineering, 60 (2013), pp. 310–320.

[4] S. M. FALZARANO AND C. MAGI-GALLUZZI, *Staging prostate cancer and its relationship to prognosis*, Diagnostic Histopathology, 16 (2010), pp. 432–438.

[5] E. J. FELEPPA, C. R. PORTER, J. KETTERLING, P. LEE, S. URBAN, AND A. KALISZ, *and Monitoring Treatment of Prostate Cancer*, 26 (2006), pp. 163–172.

[6] N. J. FITZSIMONS, J. C. PRESTI, C. J. KANE, M. K. TERRIS, W. J. ARONSON, C. L. AMLING, AND S. J. FREEDLAND, *Is biopsy Gleason score independently associated with biochemical progression following radical prostatectomy after adjusting for pathological Gleason score?*, The Journal of urology, 176 (2006), pp. 2453–8; discussion 2458.

[7] G. D. GROSSFELD, J. J. CHANG, J. M. BROERING, Y. P. LI, D. P. LUBECK, S. C. FLANDERS, AND P. R. CARROLL, *Under staging and under grading in a contemporary series of patients undergoing radical prostatectomy: results from the Cancer of the Prostate Strategic Urologic Research Endeavor database.*, The Journal of urology, 165 (2001), pp. 851–856.

[8] S. M. HAN, H. J. LEE, AND J. Y. CHOI, *Computer-aided Prostate Cancer Detection using Texture Features and Clinical Features in Ultrasound Image*, Journal of Digital Imaging, 21 (2008), pp. 121–133.

[9] A. C. HODGE, A. FENSTER, D. B. DOWNEY, AND H. M. LADAK, *Prostate boundary segmentation from ultrasound images using 2D active shape models: Optimisation and extension to 3D*, Computer Methods and Programs in Biomedicine, 84 (2006), pp. 99–113.

[10] F. IMANI, *Ultrasound-based Tissue Typing Using RF Time Series : Clinical Feasibility Studies and Applications*, PhD thesis, Queen's University, 2014.

[11] F. IMANI, B. ZHUANG, A. TAHMASEBI, J. T. KWAK, S. XU, H. AGARWAL, S. BHARAT, N. UNIYAL, I. B. TURKBEY, P. CHOYKE, P. PINTO, B. WOOD, M. MORADI, P. MOUSAVI, AND P. ABOLMAESUMI, *Augmenting MRI‚Äìtransrectal ultrasound-guided prostate biopsy with temporal ultrasound data: a clinical feasibility study*, International Journal of Computer Assisted Radiology and Surgery, 10 (2015), pp. 727–735.

[12] M. INAHARA, H. SUZUKI, H. NAKAMACHI, N. KAMIYA, M. SHIMBO, A. KOMIYA, T. UEDA, T. ICHIKAWA, K. AKAKURA, AND H. ITO, *Clinical evaluation of transrectal power doppler imaging in the detection of prostate cancer*, International urology and nephrology, 36 (2004), pp. 175–180.

[13] J. A. JENSEN, *User's guide for the Field II program*, Non-Journal Publication, (2001), pp. 1–68.

[14] E. KONOFAGOU, *Quo vadis elasticity imaging?*, Ultrasonics, 42 (2004), pp. 331–336.

[15] M. LASPINA AND G. P. HAAS, *Update on the diagnosis and management of prostate cancer*, The Canadian journal of urology, 15 Suppl 1 (2008), p. 3.

[16] R. LLOBET, J. C. PEREZ-CORTES, A. H. TOSELLI, AND A. JUAN, *Computer-aided detection of prostate cancer*, International Journal of Medical Informatics, 76 (2007), pp. 547–556.

[17] A. T. MANUAL, *iU22 Service Manual 4535 611 65643*, (2006), pp. 1–696.

[18] U. MANUAL, *SonixMDP/SP/OP Q+ Ultrasound System*.

[19] D. MARGEL, S. A. YAP, N. LAWRENTSCHUK, L. H. KLOTZ, M. HAIDER, K. HERSEY, A. FINELLI, A. R. ZLOTTA, J. TRACHTENBERG, AND N. E. FLESHNER, *Impact of multiparametric endorectal coil prostate magnetic resonance imaging on disease reclassification among active surveillance candidates: A prospective cohort study*, Journal of Urology, 187 (2012), pp. 1247–1252.

[20] M. MORADI, P. ABOLMAESUMI, AND P. MOUSAVI, *Tissue typing using ultrasound RF time series: experiments with animal tissue samples.*, Medical Physics, 37 (2010), pp. 4401–4413.

[21] M. MORADI, S. MEMBER, P. ABOLMAESUMI, D. R. SIEMENS, E. E. SAUERBREI, A. H. BOAG, P. MOUSAVI, AND S. MEMBER, *Augmenting Detection of Prostate Cancer in Transrectal Ultrasound Images Using SVM and RF Time Series*, 56 (2009), pp. 2214–2224.

[22] M. MORADI, P. MOUSAVI, AND P. ABOLMAESUMI, *Computer-aided diagnosis of prostate cancer with emphasis on ultrasound-based approaches: a review.*, Ultrasound in medicine & biology, 33 (2007), pp. 1010–28.

[23] K. R. MOREIRA LEITE, L. H. A. CAMARA-LOPES, M. F. DALL'OGLIO, J. CURY, A. A. ANTUNES, A. SAÑUDO, AND M. SROUGI, *Upgrading the Gleason score in extended prostate biopsy: implications for treatment choice.*, International journal of radiation oncology, biology, physics, 73 (2009), pp. 353–6.

[24] N. M. TOLE, *Image Characteristics in Clinical Ultrasound*, 2005.

[25] N. M. TOLE, *Interaction of Ultrasound with Matter*, 2005.

[26] N. M. TOLE, *Ultrasound beam shape.pdf*, 2005.

[27] P.-H. TSUI AND C.-C. CHANG, *Imaging local scatterer concentrations by the Nakagami statistical model.*, Ultrasound in medicine {&} biology, 33 (2007), pp. 608–619.

[28] H. G. WELCH AND W. C. BLACK, *Overdiagnosis in Cancer*, JNCI Journal of the National Cancer Institute, 102 (2010), pp. 605–613.

[29] M. ZHANG, P. NIGWEKAR, B. CASTANEDA, K. HOYT, J. V. JOSEPH, A. DI SANT'AGNESE, E. M. MESSING, J. G. STRANG, D. J. RUBENS, AND K. J. PARKER, *Quantitative Characterization of Viscoelastic Properties of Human Prostate Correlated with Histology*, Ultrasound in Medicine & Biology, 34 (2008), pp. 1033–1042.